LA-UR- 97-2778

Title: CONF-9703109--

INERTIAL CONFINEMENT FUSION AT THE LOS ALAMOS NATIONAL LABORATORY

Author(s): Erick Lindman
D. Baker, C. Barnes, B. Bauer, J. B. Beck, R. Berggren, B. Bezzerides, P. Bradley, R. E. Chrien, M. Clover, J. Cobble, C. A. Coverdale, M. Cray, N. Delamater, D. DuBois, B. H. Failor, J. C. Fernandez, L. Foreman, R. Gibson, P. Gobby, S. R. Goldman, D. Harris, A. Hauer, J. Hoffer, N. Hoffman, W. W. Hsing, R. Johnson, K. Klare, R. Kopp, W. Krauser, G. Kyrala, G. Magelssen, R. Mason, D. Montgomery, T. J. Murphy, J. Oertel, G. Pollak, H. Rose, K. Schoenberg, D. P. Smitherman, M. S. Sorem, F. Swenson, D. Tubbs, W. Varnum, H. Vu, J. Wallace, R. Watt, R. Weaver, B. Wilde, M. Wilke, D. Wilson, W. M. Wood

Submitted to: Proceedings of
The Second Symposium on Current Trends in International Fusion Research: Review and Assessment
March 10-14, 1997, Washington, D.C., U.S.A.

Los Alamos
NATIONAL LABORATORY

Form No. 836 R5
ST 2629 10/91

DISCLAIMER

INERTIAL CONFINEMENT FUSION AT THE LOS ALAMOS NATIONAL LABORATORY

Erick Lindman
D. Baker, C. Barnes, B. Bauer, J. B. Beck, R. Berggren, B. Bezzerides, P. Bradley, R. E. Chrien, M. Clover, J. Cobble, C. A. Coverdale, M. Cray, N. Delamater, D. DuBois, B. H. Failor, J. C. Fernandez, L. Foreman, R. Gibson, P. Gobby, S. R. Goldman, D. Harris, A. Hauer, J. Hoffer, N. Hoffman, W. W. Hsing, R. Johnson, K. Klare, R. Kopp, W. Krauser, G. Kyrala, G. Magelssen, R. Mason, D. Montgomery, T. J. Murphy, J. Oertel, G. Pollak, H. Rose, K. Schoenberg, D. P. Smitherman, M. S. Sorem, F. Swenson, D. Tubbs, W. Varnum, H. Vu, J. Wallace, R. Watt, R. Weaver, B. Wilde, M. Wilke, D. Wilson, W. M. Wood

Los Alamos National Laboratory
Los Alamos, NM 87545 USA

ABSTRACT

The Los Alamos National Laboratory is contributing to the resolution of key issues in the US Inertial-Confinement-Fusion Program and plans to play a strong role in the experimental program at the National Ignition Facility when it is completed.

I. INTRODUCTION

The goal of the Los Alamos Inertial-Confinement-Fusion (ICF) Program is to achieve fusion in the laboratory. And, we believe that the facility, in which this goal is most likely to be achieved, is the National Ignition Facility (NIF). The NIF {1}, which is currently scheduled for completion in 2004, is a 192-beam laser operating at 0.35 μm wavelength. It is capable of delivering 1.8 MJ to a mm size target at a peak power of 500 TW. It will be capable of direct- and indirect-drive illumination and is expected to achieve a maximum of 45 MJ of fusion yield per pulse.

Direct Drive

In direct drive the energy of the laser is deposited spherically symmetrically on the surface of the spherical capsule containing the deuterium-tritium (DT) fuel. The laser energy diffuses into the capsule and produces a region of high pressure which accelerates the outer layer outward and the inner layers inward. The inward acceleration causes the fuel in the capsule to be compressed and heated to ignition conditions. Los Alamos has a small effort in support of this approach. It is primarily directed toward the investigation of the use of foam layers on the outside of the capsule to improve the drive symmetry. Experimental results {2}and theoretical calculations {3} suggest that some improvement is achievable using foam layers.

Indirect Drive

In indirect drive the capsule is located inside a high-Z container called a hohlraum. The laser energy is deposited on the walls of the hohlraum where it is absorbed and converted to x-rays. These x-rays then carry the energy to the capsule and ignition conditions are achieved as before. The bulk of the Los Alamos program is directed towards achieving ignition with indirect drive. Since existing lasers cannot achieve the conditions expected in indirect drive targets on the NIF, it is necessary to use computer codes such as LASNEX {4} to predict the conditions that will be achieved and the subsequent behavior of the capsule and DT fuel. To check the reliability of the predictions of the code, extensive experiments are carried out in the parameter ranges accessible to existing lasers and compared to code predictions for these cases. LASNEX predictions of NIF-target behavior and comparisons of LASNEX calculations with experiments will be discussed in more detail below.

II. PREDICTIONS OF NIF-TARGET PERFORMANCE

Integrated Modeling and the LASNEX Computer Code

Integrated modeling refers to the practice of calculating all of the dynamics inside the hohlraum simultaneously, rather than calculating parts of the problem separately. Physical effects included in such calculations are (1) laser-ray propagation, refraction, absorption and x-ray conversion, (2) laser-entrance-hole (LEH) effects such as window (the thin membrane covering the LEH to hold in the gas) expansion and hole closure, (3) x-ray transport with typically 70 energy groups, (4) wall and channel plasma dynamics, spot motion, stagnation, filling and hydro coupling and (5) capsule dynamics such as preheat, implosion and burn. Physical effects that are currently not included in the calculations, because they are not in the LASNEX code, include plasma interpenetration and laser-plasma instabilities. Hydrodynamic instabilities are not included either, but for different reasons. The fine zoning required to resolve the small perturbations on the capsule which grow as the result of Rayleigh-Taylor instabilities would make the calculation prohibitively expensive to carry out. These effects are calculated with the LASNEX code in separate capsule-only calculations.

NIF-Target Calculations

Integrated modeling with the LASNEX code has been used to calculate the performance of, and demonstrate the attainment of ignition for, a variety of indirect-drive targets for the NIF. The targets consist of a gold hohlraum in which laser energy is deposited and converted to x-rays and a capsule that is imploded by the x-rays. The same hohlraum was used in all of the indirect-drive targets. It was a gold cylinder, 10 mm long by 5.5 mm in diameter, with concentric laser-entrance holes (LEH's) in the gold endcaps. The LEH's were 2.75 mm in diameter and were covered with a thin polyimide window to hold in the hydrogen-helium gas whose density was approximately 1.3 mg/cm^3. The hohlraums were then irradiated with either two or three cones of beams from either side.

The calculation of the Livermore PT (point target) design, shown in Fig. 1, was first repeated, and the results were compared to Livermore results {5-8}. The capsule in this target was a bromine-doped plastic (CH) shell with an inner radius of 0.95 mm, an outer radius of 1.1 mm and a density of 1.05 g/cm^3. A layer of deuterium-tritium (DT) ice having a density of 0.25 g/cm^3 extended from a radius of 0.87 mm to the inner radius of the plastic shell. Inside the DT-ice layer the rest of the volume is filled with DT gas at a

density of 0.3 mg/cm^3. Two cones of beams whose intensities were varied independently to achieve the required time-dependent drive and symmetry were used in the calculation. This target calculated to ignite with two-cone illumination and gave a fusion yield of 12 to 15 MJ with a laser energy of 1.3 MJ and a peak power of 360 TW.

An alternate design, also shown in Fig. 1, was then proposed at Los Alamos in which the plastic shell was replaced with a copper-doped beryllium shell {8}. All dimensions remained the same except for the outer radius of the beryllium shell which dropped slightly to 1.105 mm. Again two cones of beams whose intensities were varied independently to achieve the required time-dependent drive and symmetry were used in the calculations. This target calculated to ignite with two-cone illumination and gave a fusion yield of 16 MJ with a laser energy of 1.4 MJ and a peak power of 400 TW. The advantages of this design over the original PT design is a reduced sensitivity to the growth of surface perturbations and a reduced sensitivity to thermal errors during the process of forming and symmetrizing the DT-ice layer. The disadvantages are associated with fabrication procedures. A seamless sphere cannot be made as easily with beryllium as it can with plastic. Instead two hemispheres may have to be made and joined. In addition the beryllium capsule cannot be diffusion filled with DT. Instead it must be filled through a hole which then must be plugged. The resulting perturbations at the joint and the fill hole may lead to jetting of the beryllium into the fuel.

Ignition was achieved with another variation of the PT design involving the use of three beam cones instead of two. Drive symmetry was easier to obtain with this approach, and a fusion yield of 12 MJ was obtained with 1.3 MJ in at a peak power of 360 TW.

More recently another alternate design has been proposed at Los Alamos, a double-shell design {9}, shown in Fig. 2, whose principal advantages are that it is non-cryogenic and does not require a shaped laser pulse. Its disadvantages are lower yield and greater sensitivity to hydrodynamic instabilities. The outer shell is copper-doped beryllium with an inner radius of 0.69 mm and an outer radius of 1.11 mm. Inside of the ablator is a layer of plastic foam with density 0.05g/cm^3 which extends from a radius of 0.37 mm to 0.69 mm. This layer plays the role of a cushion allowing the imploding outer shell to smoothly accelerate the inner shell which contains the DT fuel. The inner shell is made of a gold-copper alloy with a density of 18.9 g/cm^3 and inner and outer radii of 0.34 and 0.37 mm respectively. The gaseous DT fuel is contained with the inner shell at a density of 0.1g/cm^3. When this target is driven with a 6 ns flat-top pulse at 300 TW, 1.8 MJ is delivered to the target and a calculated yield of 1.4 to 2 MJ is obtained. It is not a high-gain target, but ignition is obtained.

Pulse Shaping and Beam Phasing

In order to compress the fuel to high density and raise its temperature to the required value, it must first be adiabatically compressed and then shock heated symmetrically. The laser pulses necessary to do this, shown in Fig 3, are complicated functions of time. Significant deviation from the resulting drive will prevent ignition of the PT target.

Adequate symmetry is required as well. The laser energy is deposited in the region where the laser beam first encounters material from the hohlraum wall. Because of the blow-off of the wall, this region moves. This spot motion along with the changing relative x-ray emission intensity from the rest of the hohlraum introduces time-dependent asymmetries in the capsule drive. The laser pointing cannot be changed on these time scales, so an alternate strategy to compensate for these time-dependent asymmetries has been devised. Two cones of beams are used to give two rings of laser spots. The "center of irradiance" can then be moved towards or away from the capsule by changing the relative intensity of

these rings. This concept is called beam phasing and is used to reduce time-dependent asymmetries. Thus the sum of the intensities of the two rings determines the capsule drive, and the difference is used to control time-dependent symmetry.

The laser power levels that were used in the calculations of the PT target are shown in Fig. 3. A measure of the drive symmetry with and without beam phasing is presented as well. The improvement in drive symmetry with beam phasing is quite apparent. If the calculation with beam phasing is repeated without beam phasing, i.e. with the total power unchanged and the ratio of the powers in the inner and outer cone held constant, the PT target does not ignite {5-8}. This result is true for the beryllium target as well. When three-cone illumination is employed, beam phasing is not required to obtain ignition. However, in the absence of beam phasing the target is much more sensitive to tiny errors in pointing and beam intensity.

Neither beam phasing nor a special laser pulse is required to obtain ignition in the double-shell target {9}. The previously quoted results were obtained with a 6-ns flat-top pulse, shown in Fig. 2, with a fixed power ratio between the inner and outer cones. The smooth acceleration of the inner shell, driven by the rising pressure in the cushion material between the shells, plays the same role as the shaped laser pulse required for the PT target.

Hydrodynamic Instabilities and Surface Irregularities

The LASNEX code can also be used to perform direct-numerical-simulation (DNS) calculations of the growth of perturbations from fabrication surface irregularities {10}. Accurate calculations of these effects are not included in integrated-modeling calculations because the zoning requirements exceed the capacity of the computer. Instead they are evaluated in separate capsule-only calculations in which high resolution is obtained by putting all the zones in the capsule.

Many spherical-harmonic modes can then be included in the calculation simultaneously. No adjustable model parameters are used, and the initial amplitudes are chosen to represent a spectrum measured from capsules that were made using state-of-the-art technology. The finite initial amplitudes lead to nonlinear growth, and the shape of the imploded fuel and its self-consistent yield are obtained.

Initial DNS calculations for NIF suggest that both the beryllium and the plastic capsules tolerate ablator roughness up to 40 nm. Fig. 4 shows yield plotted against surface roughness for a series of such calculations. At 40 nm surface roughness the yields have dropped by only as much as 10%, while at 50 nm the capsules no longer ignite. For plastic capsules 20 nm surface roughness is attainable with current state-of-the-art fabrication techniques.

The other surface which has been studied in some detail is the inner DT-ice surface. Here two dimensional multimode calculations show that the beryllium capsule tolerates greater DT-ice surface roughness than the plastic capsule. Fig. 5 shows yield plotted against ice-surface roughness for the two capsules. The plastic capsule fails to ignite at a surface roughness of 2 μm, while the beryllium capsule is still showing 5 MJ of yield at 8 μm. Using a process called beta layering, DT-ice layers can be formed inside a capsule with surface roughnesses less than 2 μm.

III. EXPERIMENTS AND FUTURE RESEARCH

Experiments are being carried out in a number of different areas to increase our understanding of the physical processes occurring in these hohlraums and to verify the accuracy of our code predictions. One such area which will not be discussed in detail is that of laser-plasma instabilities {11-21}. In this area questions currently being addressed include: What saturates stimulated Brillouin scattering? And can we limit stimulated Brillouin (SBS) and stimulated Raman (SRS) scattering for relevant NIF plasma conditions? The answers to these questions will give us more confidence in our ability to predict backscatter levels on the NIF. Other areas of current research, that will be discussed in detail, include drive symmetry, hydrodynamic instabilities and beta layering.

Drive Symmetry

The discrepancies between Nova experiments in vacuum and gas-filled hohlraums, shown in Fig. 6, and LASNEX modeling of capsule-implosion symmetry in gas-filled hohlraums were first reported in 1994 {22} and are now well established {23-28}. A number of physical mechanisms which might contribute to these effects have been evaluated {29,30}. One of these is currently thought to be responsible for essentially all of the effect on capsule-implosion symmetry. This mechanism, laser-beam propagation in filaments bent by plasma flow, is being studied intensively at Los Alamos {30} and Livermore {31}, and a bending of the laser beam by as much as 9 degrees has been theoretically predicted under idealized conditions {31}.

The strongest evidence for the conclusion that "beam steering" is the dominant effect on capsule-implosion symmetry, however, comes from recent calculations of Nova experiments. Using thin-wall hohlraums in Nova experiments (150 micron thick epoxy cylinders with 2 microns of Au deposited on the inner surface), it is possible to see through the walls of the hohlraum with gated x-ray imagers and see the location of the laser spots as a function of time. This diagnostic can be simulated in LASNEX calculations to get the equivalent spot motion.

The spot shifts seen in experiments differ by as much as 300 microns from those seen in calculations when no additional deflection is included. The X's in Fig. 7 show the shift in the location of the hot spot from nominal pointing in a recent Nova shot as a function of time. When a LASNEX calculation with no additional deflection is done, some spot motion occurs because of the wall motion. The spot shift as a function of time for this case is given by the dotted curve in Fig. 7. The disagreement between experiment and calculation is thought to result from bending of the laser beam by the plasma {30,31}. The effect is strongest at a point in the plasma where the transverse Mach number of the flow is one and is a complicated function of the local plasma parameters.

The effect can be mocked up in LASNEX calculations, however, by bringing the laser beam in at a different angle as shown in Fig. 8. The bottom half of the Figure shows the laser beam propagating at 50 degrees from the hohlraums axis as they do at Nova. The upper half of the Figure shows a laser beam that is propagating at 58.75 degrees through the same intersection point with the hohlraum axis. The laser spot is shifted roughly 20 microns per degree or approximately 175 microns. This angle is changed in the calculation as a function of time to give the time dependence shown in the dashed curve in Fig. 9. The resulting spot shift, shown in the dash-dot curve in Fig. 7, matches the experimental data quite well over the early part of the time interval. The discrepancy at late time is thought to be due to an artifact in the experimental data reduction.

When the additional angular deflection is included in the calculation in such a way as to match the spot motion seen in the experiment, the imploded-capsule symmetry agrees well with the experimental data. Figure 9 shows experimental data and calculations for a pointing scan at Nova in which the length of the hohlraum and the laser pointing were varied simultaneously. The distortion is the ratio of the length of the semi-major axis of the ellipsoid transverse to the hohlraum axis divided by the length of the semi-major axis along the hohlraum axis. The laser pointing is defined here as the distance from the center of the hohlraum to the intersection of the central ray of the laser beam with the hohlraum's axis, and the length of the hohlraum is always adjusted so that this intersection is in the plane of inside surface of the laser-entrance hole. The symmetry of the imploded capsule changes from prolate (sausage) at inner pointing at the left to oblate (pancake) at outer pointing at the right. The discrepancy between the experimental data and LASNEX calculation is quite apparent. When the calculation is done with the additional angular deflection, however, the resulting distortion of the imploded capsule is consistent with the experimental values.

Smoothing the beams using random phase plates or kineform phase plates is expected to reduce this problem substantially. Preliminary results from ongoing experiments seem to confirm this hypothesis. Physics packages which could calculate these effects have not been added to LASNEX. If beam smoothing eliminates these effects, there will be little interest in adding the additional physics packages to LASNEX.

Hydrodynamic Instabilities

Indirect-drive Rayleigh-Taylor experiments in a cylindrical geometry are being carried out at Nova by Los Alamos investigators {32-36}. The use of a cylindrical geometry retains convergent effects while providing diagnostic access to the inside surface. These experiments are an important check on the planar Rayleigh-Taylor experiments which have been carried out by others. In a converging geometry the mode numbers of the perturbations are conserved and the wavelengths change. As a result the growth rates change with radius and simple exponential growth is not expected. In addition growth in amplitude can occur from convergence alone. These effects are included in LASNEX calculations which agree well with the experimental results.

A typical experimental arrangement is shown in Fig. 10. A cylindrical scale-1 hohlraum is driven by 8 of the 10 Nova beams. The cylindrical implosion structure is located at the center of the main hohlraum with its axis perpendicular to the axis of the main hohlraum. One of the unused beams is used to irradiate the backlighter. A time-resolved x-ray pinhole camera is then used to record images of the imploding cylindrical structure.

Experimental data from a recent experiment {36} is shown in Fig. 11. This experiment was designed to measure the feedthrough of a perturbation imposed on the outer surface of a cylindrical shell to its inner surface and its subsequent growth. The initial target was a 40 μm thick plastic shell with an inner diameter of 430 μm. It had a 4 μm thick layer of chlorinated plastic on its inner surface to act as a marker layer by absorbing x-rays. Its interior was filled with plastic foam, and it had an m=12 perturbation machined onto the outer surface with a peak-to-valley ratio of 9 μm. In Fig. 11 at 2.11 ns the black marker layer in the images has expanded to a thickness of about 20 μm and shows structure which came from the perturbation machined onto the outer surface of the plastic shell. At later time the growth of these perturbations is seen as the shell decelerates because of the pressure buildup in the foam inside the shell.

A control experiment, in which no perturbation was machined on the outer surface of the cylindrical shell, was performed for comparison. A single image from this latter experiment is shown at the bottom of Fig. 11. The marker layer in it shows no m=12 structure as expected. LASNEX calculations of these experiments reproduce these images quite well.

Beta Layering

NIF ignition designs employ uniform spherical layers of cryogenic fuel. The preferred mechanism for producing such layers in capsules filled with DT gas, and subsequently cooled, is called beta layering. It uses re-absorption of the β emission from the tritium in the DT fuel to drive an ice layer to uniformity. Optimization of this mechanism for different capsule designs is currently an active area of research at Los Alamos{37-40}.

The beta-layering procedure begins with the freezing of the fuel inside a capsule into an irregular mass. The self-heated DT then establishes a parabolic radial temperature profile. The temperature of the outer surface is held approximately constant by the continuous heat extraction. As a result the temperature of the inner surface varies with the radial thickness of the layer: the thicker the layer, the warmer the surface. DT sublimes from the thick regions to re-freeze at the thin regions. Layer uniformity increases 10-fold every 61 minutes. The interior surface reaches equilibrium when it follows an isotherm. Since the interior isotherm will be concentric to the external surface at equilibrium, the interior surface of the DT fuel will be concentric and uniform as well.

An rms. roughness of the order of 2 μm is typically seen in experiments. The measured power spectrum {39,40} of a 139 μm thick layer at 18.8K is shown in Fig. 12. The roughness as a function of spherical-harmonic mode number shows the largest contribution at low mode number with a dramatic decrease at high mode number. Two-dimensional realizations of spectra such as this are used in the DNS calculations mentioned earlier. These data plus the calculations support the contention that ignition is achievable on the NIF.

IV. CONCLUSIONS

The National Ignition Facility will be an important research facility for the study of fusion energy, astrophysical phenomena, plasma physics, atomic physics and hydrodynamics. It will, indeed, become the center for research in many of these areas. Researchers from laboratories and universities in the United States and from around the world will be able to participate in projects that can not be done elsewhere.

Every effort is being made to assure the achievement of ignition at the National Ignition Facility. Research workers at Los Alamos are contributing extensively to this effort. Researchers at Los Alamos and elsewhere look forward to playing a strong role in the research work that will be performed at the National Ignition Facility when it is complete.

Work performed for the U. S. Department of Energy under Contract No. W--7405--ENG--36.

REFERENCES

{1} "National Ignition Facility Conceptual Design Report," Lawrence Livermore National Laboratory Proposal, UCRL-Prop-117093, NIF-LLNL-94-113, L-16973, August 1994.

{2} R. G. Watt, D. C. Wilson, R. E. Chrien, R. V. Hollis, P. L. Gobby, R. J. Mason R. A. Kopp, R. A. Lerche, D. H. Kalantar, B. MacGowan, B. B. Nelson, P. W. McKenty and O. Willi, "Foam Buffered Spherical Implosions at 527 nm," to be published in Physics of Plasmas.

{3} R. J. Mason, R. A. Kopp, H. X. Vu, D. C. Wilson, S. R. Goldman, R. G. Watt, M. Dunne and O. Willi, "Computational Study of Laser Imprint Mitigation in Foam-Buffered ICF Targets," to be published in Physics of Plasmas.

{4} G. B. Zimmerman and W. L. Kruer, Comments Plas. Phys. 2, 51 (1975).

{5} S. W. Haan and S. M. Pollaine, "Target Design for Laser-Driven Thermonuclear Fusion," LLNL Research Monthly 93-1,5 (1993) (unpublished).

{6} S. W. Haan, S. M. Pollaine, J. D. Lindl, L. J. Suter, R. L. Berger, L. V. Powers, W. E. Alley, P. A. Amendt, J. A. Futterman, W. K. Levedahl, M. D. Rosen, D. P. Rowley, R. A. Sacks, A. I. Shestakov, G. L. Stroebel, M. Tabak, S. V. Weber, G. B. Zimmerman, W. J. Krauser, D. C. Wilson, S. Coggeshall, D. B. Harris, N. M. Hoffman, and B. H. Wilde, Phys. Plasmas 2, (6), 2480 (1995).

{7} W. J. Krauser, N. M. Hoffman, D. C. Wilson, B. H. Wilde, W. S. Varnum, D. B. Harris, F. J. Swenson, P. A. Bradley, S. W. Haan, S. M. Pollaine, A. S. Wan, J. C. Moreno and P. A. Amendt, Phys. Plasmas 3, 2084 (1996).

{8} W. J. Krauser, B. H. Wilde, D. C. Wilson, P. A. Bradley, and F. J. Swenson, Proc. 12th Int. Conf. on Laser Interaction and Related Plasma Phenomena, 369, (AIP Press, 1996) p. 186.

{9} D. B. Harris and W. S. Varnum, Bull. Am. Phys. Soc. 41, 1479 (1996).

{10} N. M. Hoffman, D. C. Wilson, W. S. Varnum, W. J. Krauser and B. H. Wilde, Proc. 12th Int. Conf. on Laser Interaction and Related Plasma Phenomena, 369, (AIP Press, 1996) p. 166.

{11} B. S. Bauer, R. P. Drake, K. G. Estabrook, J. F. Camacho, R. G. Watt, M. D. Wilke, B. E. Busch and S. E. Caldwell, Phys. Plasmas 2, 2207 (1995).

{12} B. S. Bauer, R. P. Drake, K. G. Estabrook, R. G. Watt, M. D. Wilke and S. A. Baker, Phys. Rev. Lett. 74, 3604 (1995).

{13} J. Cobble, J. C. Fernandez, B. H. Wilde, S. Evans, J. Jimerson, J. Oertel, D. S. Montgomery, and C. C. Gomez, Rev. Sci. Instrum. 66, 4204 (1995).

{14} R. P. Drake, R. G. Watt and K. G. Estabrook, Phys. Rev. Lett. 77, 79 (1996).

{15} B. Bezzerides, H. X. Vu and J. M. Wallace, Phys. Plasmas 3, 1073 (1996).

{16} H. X. Vu, J. Comp. Phys. 124, 417 (1996).

{17} J. C. Fernandez, J. A. Cobble, B. H. Failor, W. W. Hsing, H. A. Rose, B. H. Wilde, K. S. Bradley, P. L. Gobby, R. Kirkwood, H. N. Kornblum, D. S. Montgomery and M. D. Wilke, Phys. Rev. E 53, 2747 (1996).

{18} J. C. Fernandez, J. A. Cobble, B. H. Failor, D. F. DuBois, S. S. Montgomery, H. A. Rose, H. X. Vu, B. H. Wilde, M. D. Wilke and R. E. Chrien, Phys. Rev. Lett. 77, 2702 (1996).

{19} H. A. Rose, Phys. Plasmas 2, 2216 (1995).

{20} R. G. Watt, J. Cobble, D. F. DuBois, J. C. Fernandez, H. A. Rose, R. P. Drake and B. S. Bauer, Phys. Plasmas 3, 1091 (1996).

{21} B. H. Wilde, J. C. Fernandez, W. W. Hsing, J. A. Cobble, N. D. Delamater, B. H. Failor, W. J. Krauser, and E. L. Lindman, Proc. 12th Int. Conf. on Laser Interaction and Related Plasma Phenomena 369, (AIP Press, 1996) p. 255.

{22} E. L. Lindman, N. Delamater, G. Magelssen and A. Hauer, Laser Interaction with Matter, Proc. 23rd European Conf. (IOP Press, 1995) p. 329.

{23} N. D. Delamater, T. J. Murphy, A. A. Hauer, R. L. Kauffman, A. L. Richard, E. L. Lindman, G. R. Magelssen, B. H. Wilde, D. B. Harris, B. A. Failor, J. Wallace, L. V. Powers, S. M. Pollaine, L. J. Suter, R. Chrien, T. D. Shepard, H. A. Rose, E. A. Williams, M. B. Nelson, M. D. Cable, J. B. Moore and K. Gifford, Phys. Plasmas 3, 2022 (1996).

{24} N. D. Delamater, T. J. Murphy, A. A. Hauer, R. L. Kauffman, A. L. Richard, E. L. Lindman, G. R. Magelssen, B. H. Wilde, D. B. Harris, B. A. Failor, J. Wallace, L. V. Powers, S. M. Pollaine, L. J. Suter, R. Chrien, T. D. Shepard, H. A. Rose, E. A. Williams, M. B. Nelson, M. D. Cable, J. B. Moore, and K. Gifford, Proc. 12th Int. Conf. on Laser Interaction and Related Plasma Phenomena 369, (AIP Press, 1996).

{25} N. D. Delamater, G. R. Magelssen and A. A. Hauer, Phys. Rev. E 53, 5240 (1996).

{26} A. A. Hauer, N. D. Delamater, E. L. Lindman, G. R. Magelssen, T. J. Murphy, H. A. Rose, et al., Proc. 24th Eur. Conf. on Laser Interaction with Matter, Madrid, Spain, 1996.

{27} A. A. Hauer, N. D. Delamater, D. Ress, W. Hsing, L. Suter, L. Powers, O. Landen, D. Harris, R. Thiessen, G. Magelssen, E. Lindman, D. Phillion, P. Amendt, R. Watt and B. Hammel, Rev. Sci. Instrum. 66, 672 (1995).

{28} A. A. Hauer, L. Suter, N. Delamater, D. Ress, L. Powers, G. Magelssen, D. Harris, O. Landen, E. Lindman, W. Hsing, D. Wilson, P. Amendt, R. Thiessen, R. Kopp, D. Phillion, B. Hammel, D. Baker, J. Wallace, R. Turner, M. Cray, R. Watt, J. Kilkenny and J. Mack, Phys. Plasmas 2, 2488 (1995).

{29} E. L. Lindman, G. R. Magelssen, S. M. Pollaine, L. V. Powers, N. D. Delamater, T. J. Murphy, B. H. Wilde, L. J. Suter, A. A. Hauer and R. L. Kauffman, Proc. 12th Int. Conf. on Laser Interaction and Related Plasma Phenomena 369, (AIP Press, 1996) p. 263.

{30} H. A. Rose, Phys. Plasmas 3, 1709 (1996).

{31} D. E. Hinkel, E. A. Williams and C. H. Still, Phys. Rev. Lett. 77, 1298 (1996).

{32} J. B. Beck, W. W. Hsing, N. M. Hoffman and C. K. Choi, Proc. 12th Int. Conf. on Laser Interaction and Related Plasma Phenomena 369, (AIP Press, 1996) p. 160.

{33} R. E. Chrien, C. W. Barnes, W. W. Hsing, G. T. Schappert, N. M. Hoffman, J. B. Beck, G. R. Magelssen, and D. P. Smitherman, Proc. 24th Eur. Conf. on Laser Interaction with Matter, Madrid, Spain, 1996.

{34} N. M. Hoffman, F. J. Swenson, W. S. Varnum, D. C. Wilson, C. W. Barnes, J. B. Beck, C. K. Choi, R. E. Chrien, W. W. Hsing, G. R. Magelssen, G. T. Schappert and D. P. Smitherman, Proc. 24th Eur. Conf. on Laser Interaction with Matter, Madrid, Spain, 1996.

{35} W. W. Hsing, C. W. Barnes, J. B. Beck, N. M. Hoffman, D. Galmiche, A. Richard, J. Edwards, P. Graham, S. Rothman and B. Thomas, Phys. Plasmas 5, (5) (1997).

{36} W. W. Hsing and N. M. Hoffman, Phys. Rev. Lett., to be published (1997).

{37} J. K. Hoffer in Laser Plasma Interactions 5: Inertial Confinement Fusion, ed. M. B. Hooper (IOP Press, 1995) p. 209.

{38} K. Hoffer, L. R. Foreman, J. J. Sanchez, E. Mapoles and J. D. Sheliak, to be published in Proc. 12th Topical Mtg. on Fusion Technology, Reno, NV (1996).

{39} J. D. Sheliak, J. K. Hoffer, L. R. Foreman and E. R. Mapoles, Fus. Tech. 30, 83 (1996).

{40} E. R. Mapoles, J. Sater, J. Pipes and E. Monsler, Phys. Rev. E 55, 3473 (1997).

FIGURE CAPTIONS

Figure 1. Calculated performance of the Livermore PT (point target) and the Los Alamos beryllium-ablator capsule designs. The results for the two capsules were obtained in calculations using the same hohlraum and laser-beam pointing.

Figure 2. Calculated performance of the Los Alamos double-shell capsule design. The results were obtained using the same hohlraum and laser-beam pointing that was used in Figure 1. The simple laser pulse shown here with no beam phasing was used in place of the tailored pulse.

Figure 3. Beam phasing. The power vs. time for the inner and outer beam cones are plotted on the same graph and compared to the total power. The flux on the capsule as a function of the polar angle is shown at different times. Data such as this are used to generate the coefficient of the Legendre function, P_2, in an expansion of the drive vs. polar angle. Typical values of P_2 as a function of time are shown for cases with and without beam phasing.

Figure 4. Calculated yield vs. ablator surface roughness. Initial DNS calculations for NIF suggest that both the beryllium and plastic capsules tolerate ablator roughness up to 40 nm.

Figure 5. Calculated yield vs. DT-ice surface roughness. 2-D multimode calculations show that the Beryllium capsule tolerates greater DT-ice surface roughness than the plastic capsule.

Figure 6. Experimentally measured capsule-implosion symmetry in vacuum and gas-filled hohlraums. As the laser pointing is varied, the imploded-capsule shape changes from prolate to oblate. If the hohlraum is filled with gas, the laser beam does not travel in a straight line. The change in the laser spot locations caused by the gas produces a different symmetry compared to vacuum for the same initial pointing.

Figure 7. Spot motion in gas-filled hohlraums. Spot motion can be measured in gas-filled thin-wall hohlraums at Nova. The observed shift in a LASNEX calculation with no externally applied additional deflection disagrees with experiment. The additional shift can be added by changing the laser propagation angle as a function of time. The added angular deflection produces a shift with deflection which agrees with the Nova spot-position data at early time.

Figure 8. Raytrace with and without added deflection. In the lower half hohlraum, the laser is propagating initially at 50° to the axis of the hohlraum as the Nova beams are designed to do. In the upper hohlraum the central ray intersects the axis of the hohlraum at the same point but the initial angle of propagation of the beam has been rotated 8.75° to approximate the additional beam deflection required at early time to match the experimentally measured hot-spot position.

Figure 9. Measured and calculated capsule-implosion symmetry. In gas filled hohlraums the calculated imploded-capsule symmetry differs from experimental measurements and is much closer to the experimental data for vacuum hohlraums. However, when the laser propagation angle in the LASNEX calculation is adjusted to reproduce the spot motion observed in a gas-filled hohlraum, the calculated imploded-capsule symmetry (plotted with T in the figure) agrees with experiment.

Figure 10. Experimental layout for Rayleigh-Taylor experiments in a cylindrical geometry. The cylindrical structure to be imploded is placed in the main hohlraum with its axis at right angles to the axis of the main hohlraum. Eight beams are used to illuminate the hohlraum and a ninth is used to illuminate the backlighter.

Figure 11. A sequence of gated X-ray images of the cylindrical backlit implosion. Emission appears on center at 2.30 ns, which is when the shock wave converges at the origin. The backlighter spatial extent is limited by the 400-μm-diameter circular apertures at each end of the cylinder, and the deviation from circularity is a measure of the effect of parallax. Shown in the bottom panel is an image of an imploding shell with no initial perturbations.

Figure 12. DT ice layer roughness characterized in spherical harmonics. Surface roughness is measured with and without a layer of DT-ice. The surface roughness of the cell in which the measurement is taken is negligible compared to the surface roughness of the DT ice when it is present.

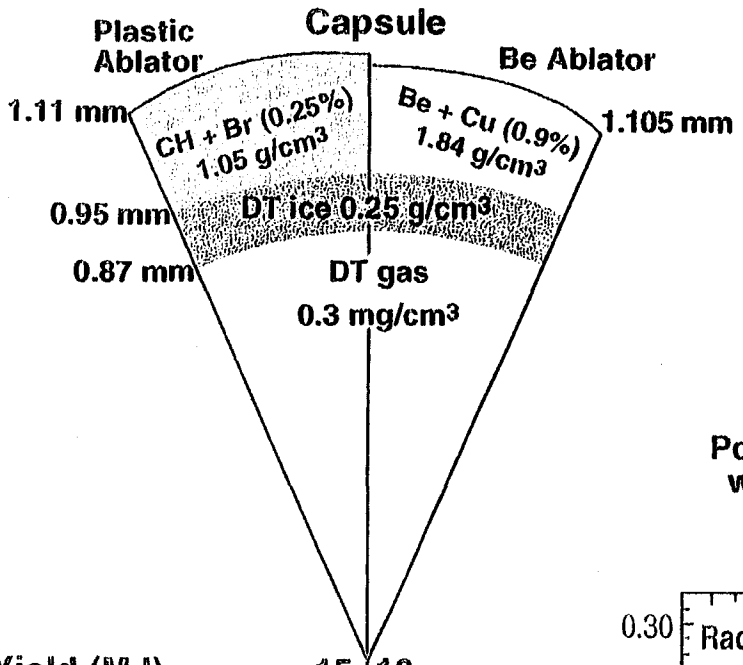

1-D Yield (MJ)	15	18
Absorbed energy (KJ)	150	200
Convergence Ratio	36	28

Gas-filled, gold-walled hohlraum driven by 192 laser beams (1.8 MJ, 500 TW) arrayed in "Inner" and "Outer" cones

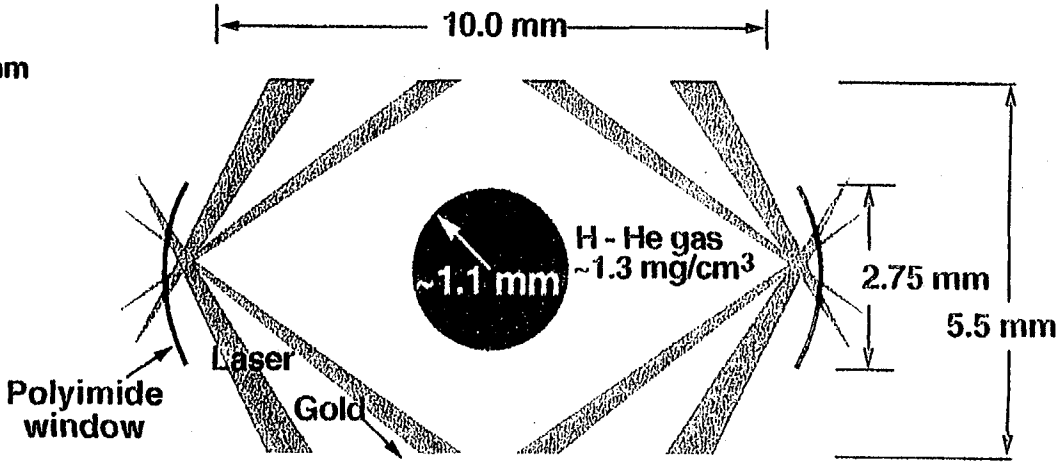

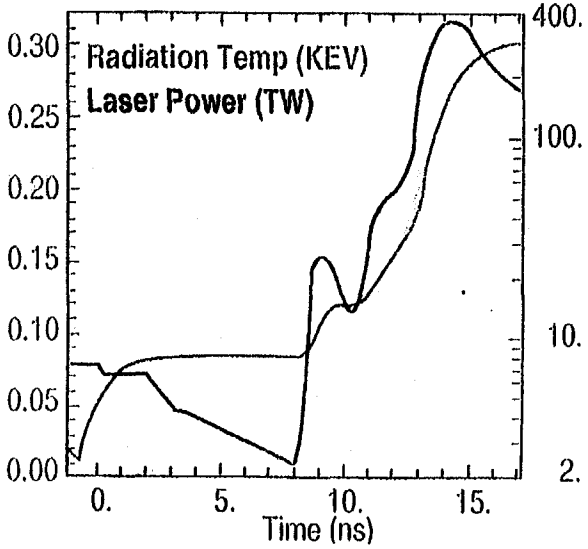

Plastic Ablator

Standard NIF hohlraum

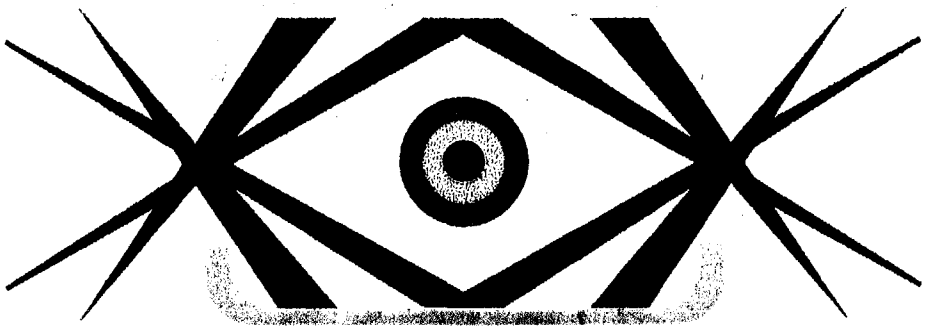

E_L ~ 1.8 MJ, P_L ~ 300 TW

Laser Pulse Shape

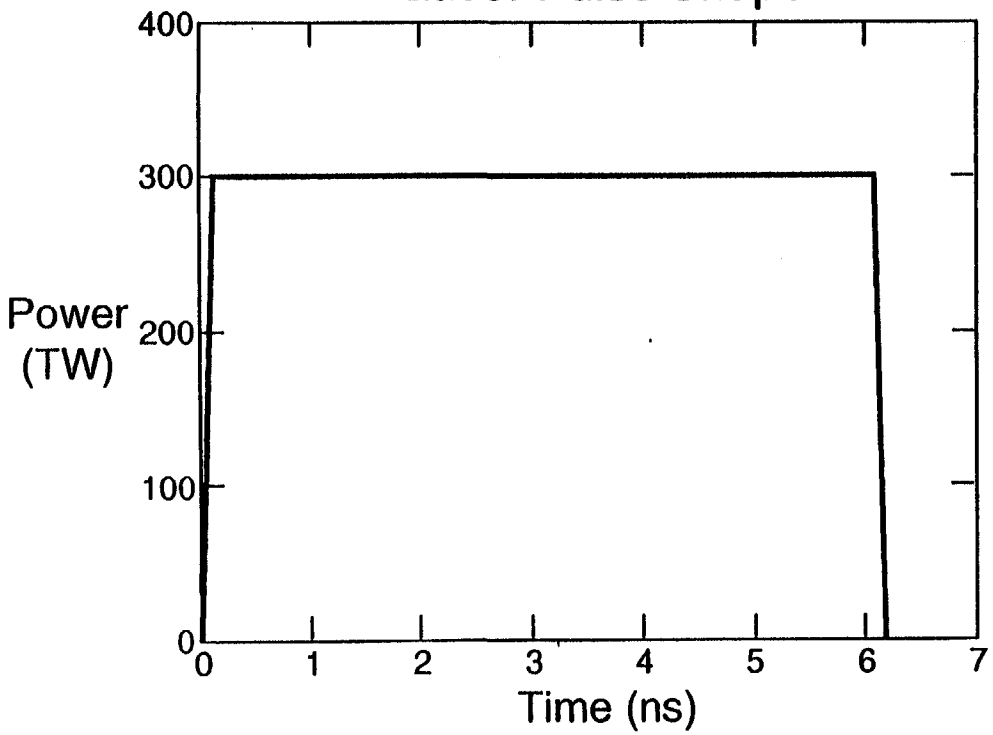

Double-shell capsule non-cryogenic

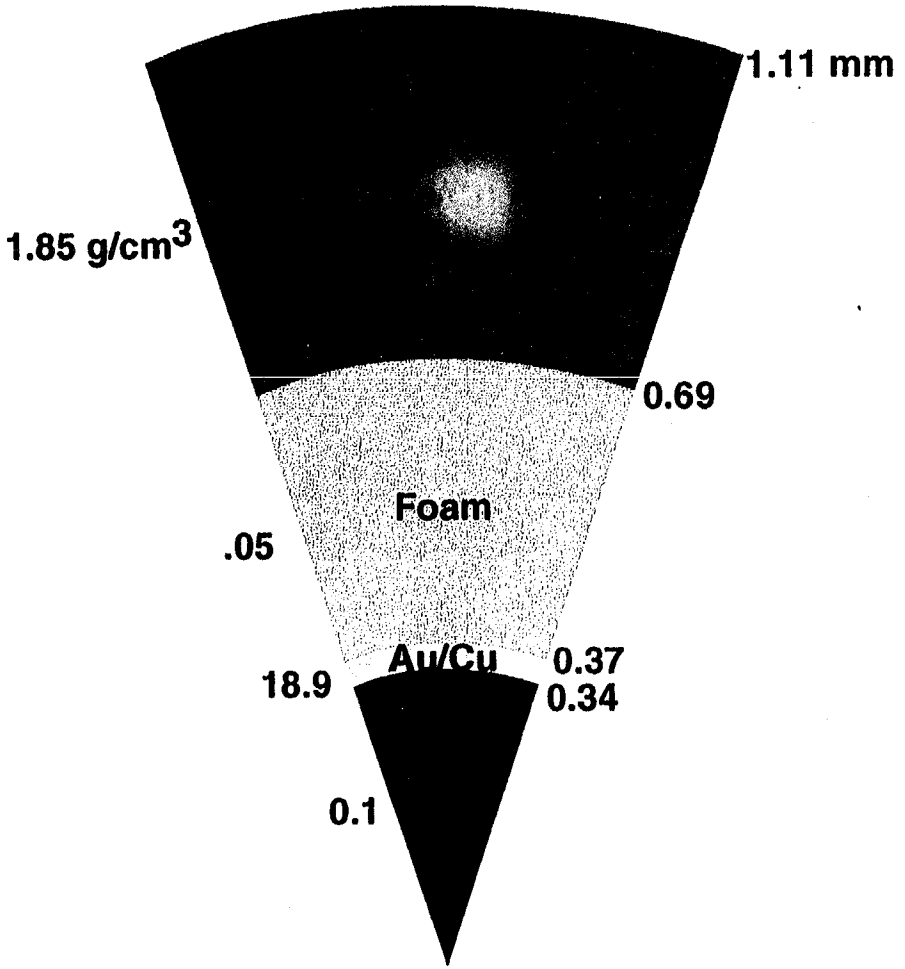

Y_{1D} ~ 2.5 MJ
Y_{2D} ~ 1.4-2.0 MJ

Hohlraum with inner and outer cones

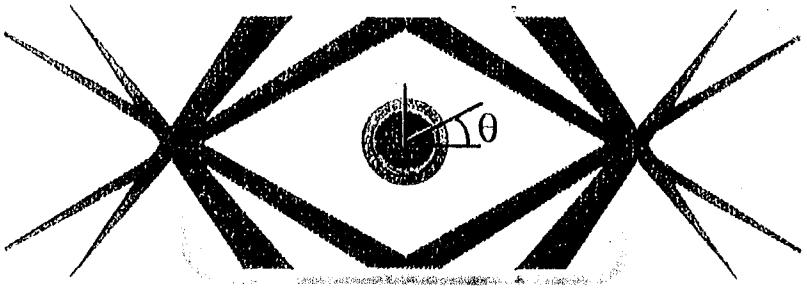

Laser power levels

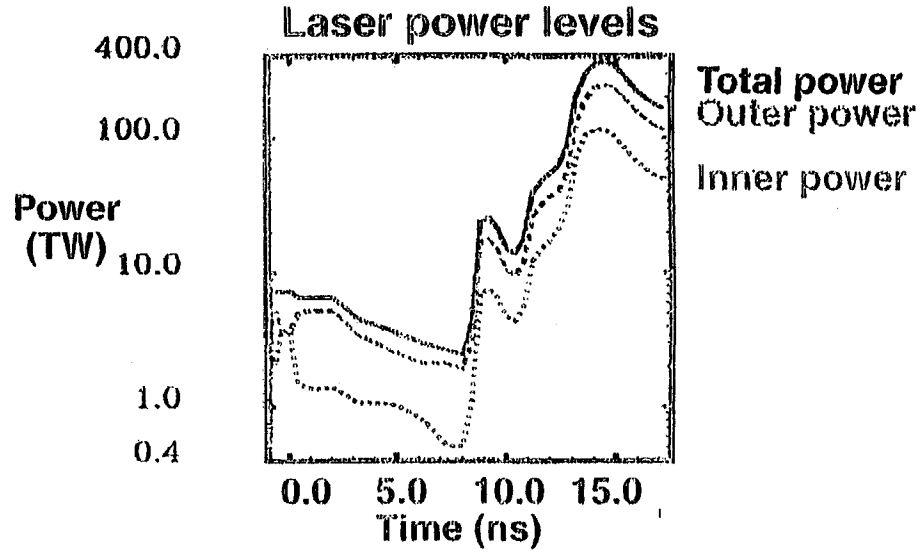

Capsule flux at different times

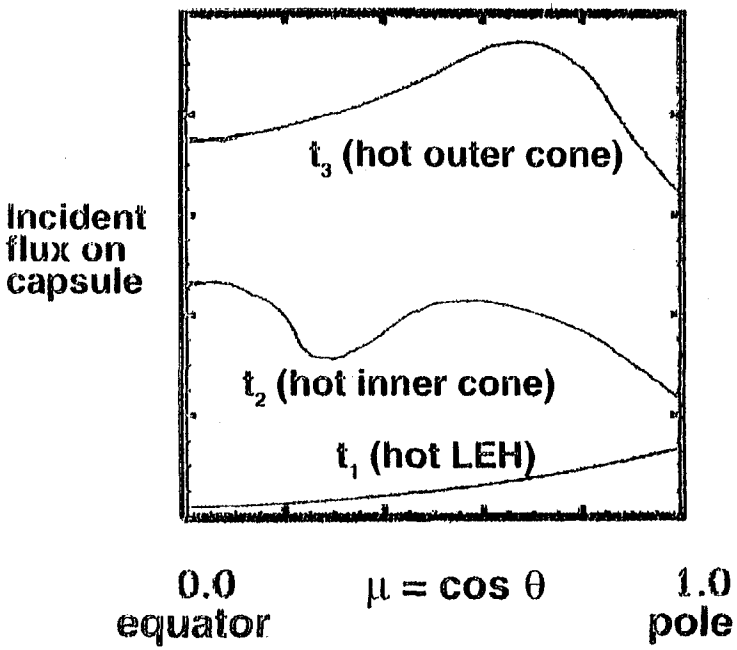

Expand flux in Legendre polynomials

Second moment of incident radiation flux

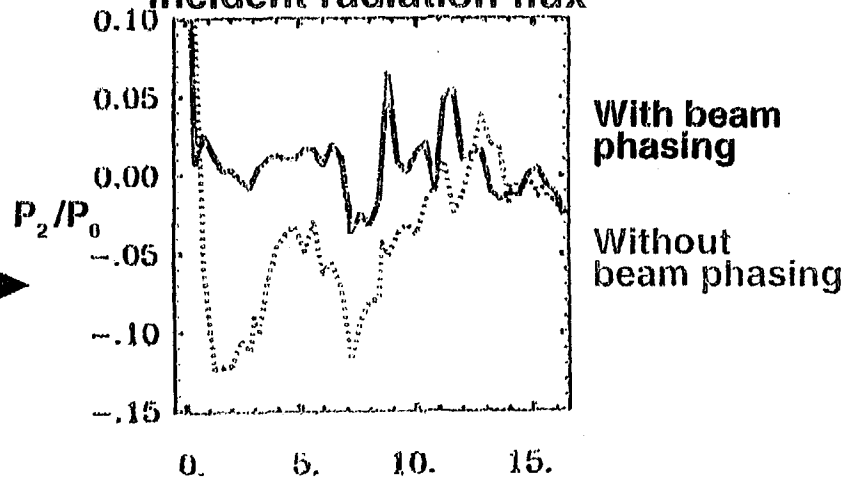

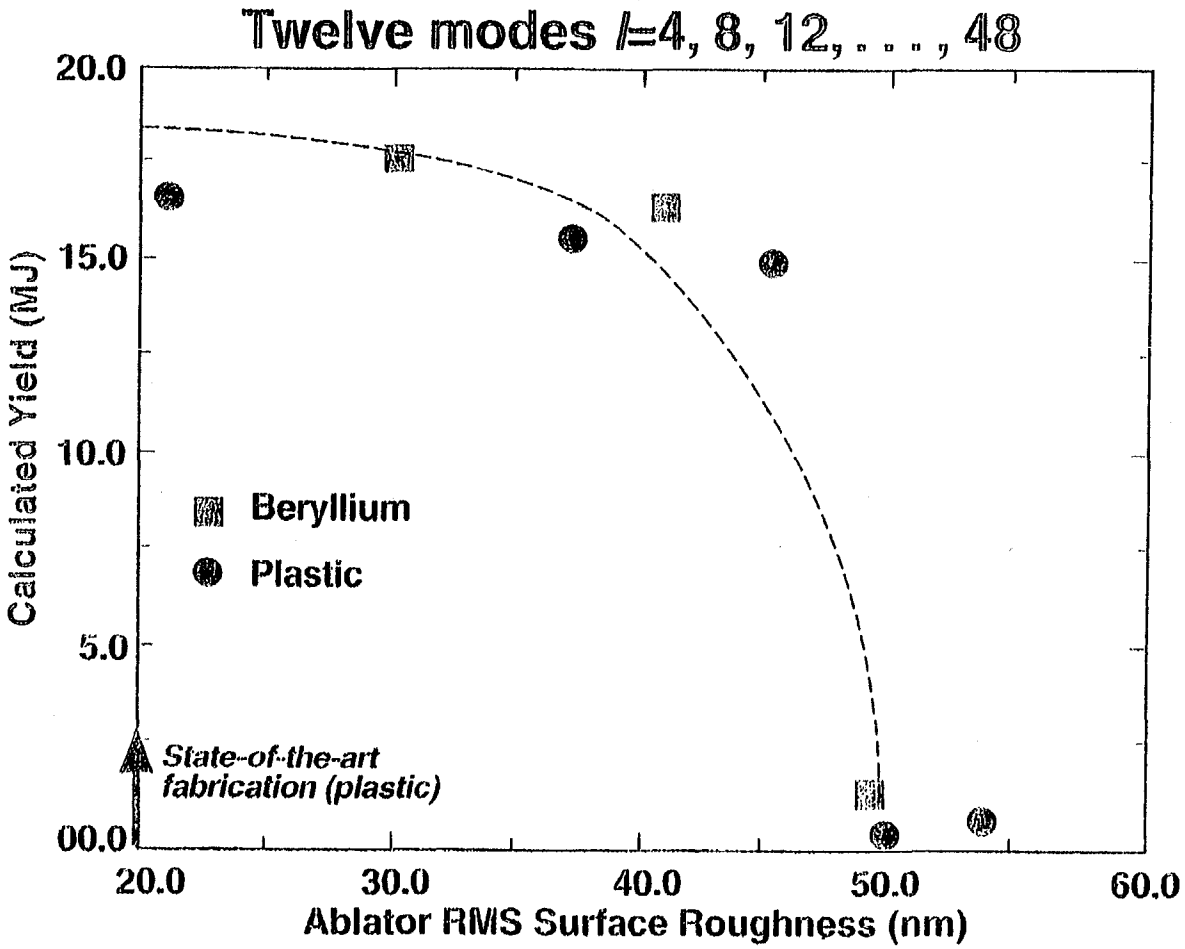
Twelve modes l=4, 8, 12, . . . , 48
20.0
15.0
10.0
5.0
00.0
Calculated Yield (MJ)
Beryllium
Plastic
State-of-the-art
fabrication (plastic)
20.0
30.0
40.0
50.0
60.0
Ablator RMS Surface Roughness (nm)

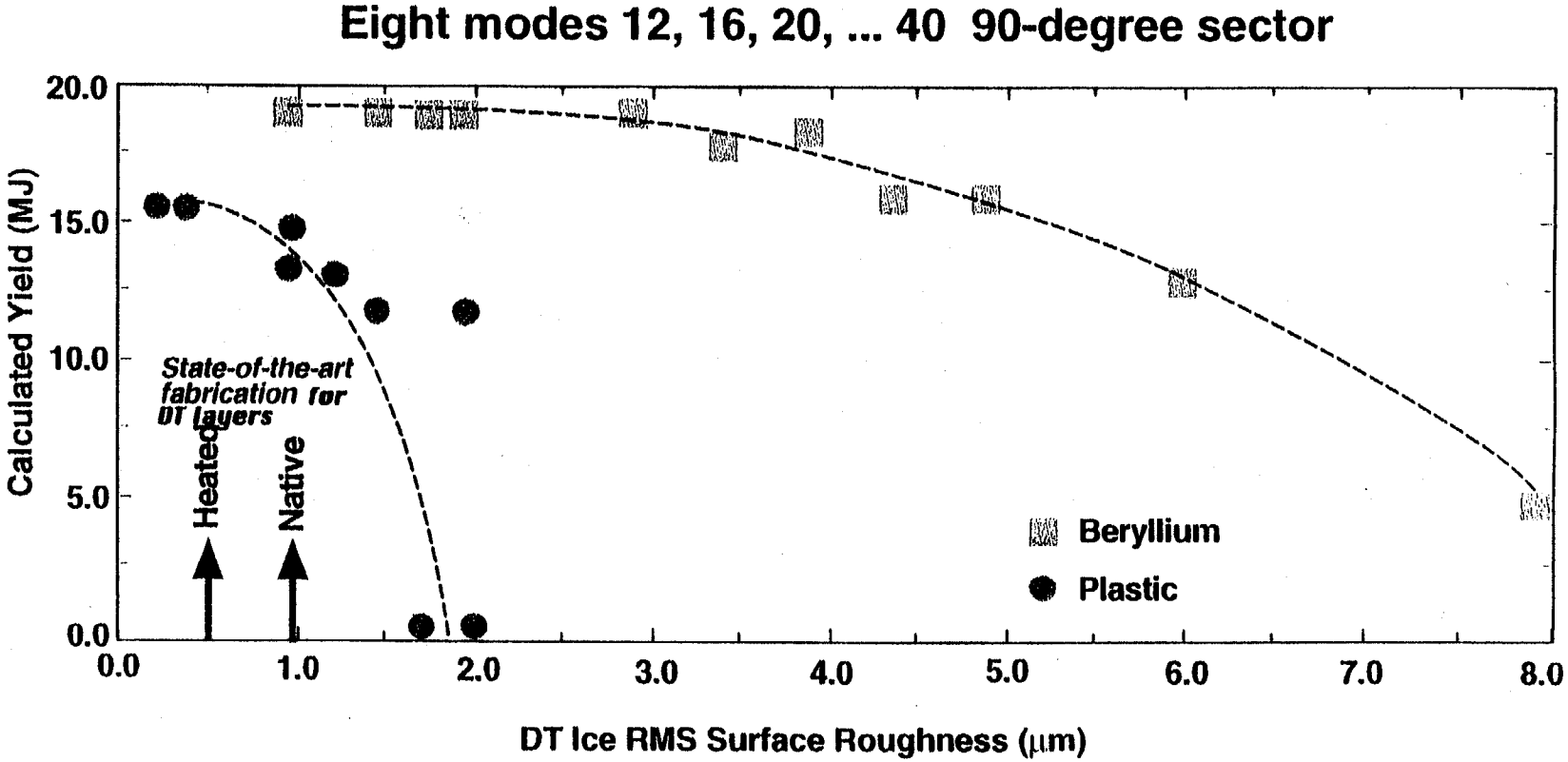
Eight modes 12, 16, 20, ... 40 90-degree sector
Calculated Yield (MJ)
20.0
15.0
10.0
5.0
0.0
0.0
1.0
2.0
3.0
4.0
5.0
6.0
7.0
8.0
DT Ice RMS Surface Roughness (μm)
State-of-the-art fabrication for DT layers
Heated
Native
Beryllium
Plastic

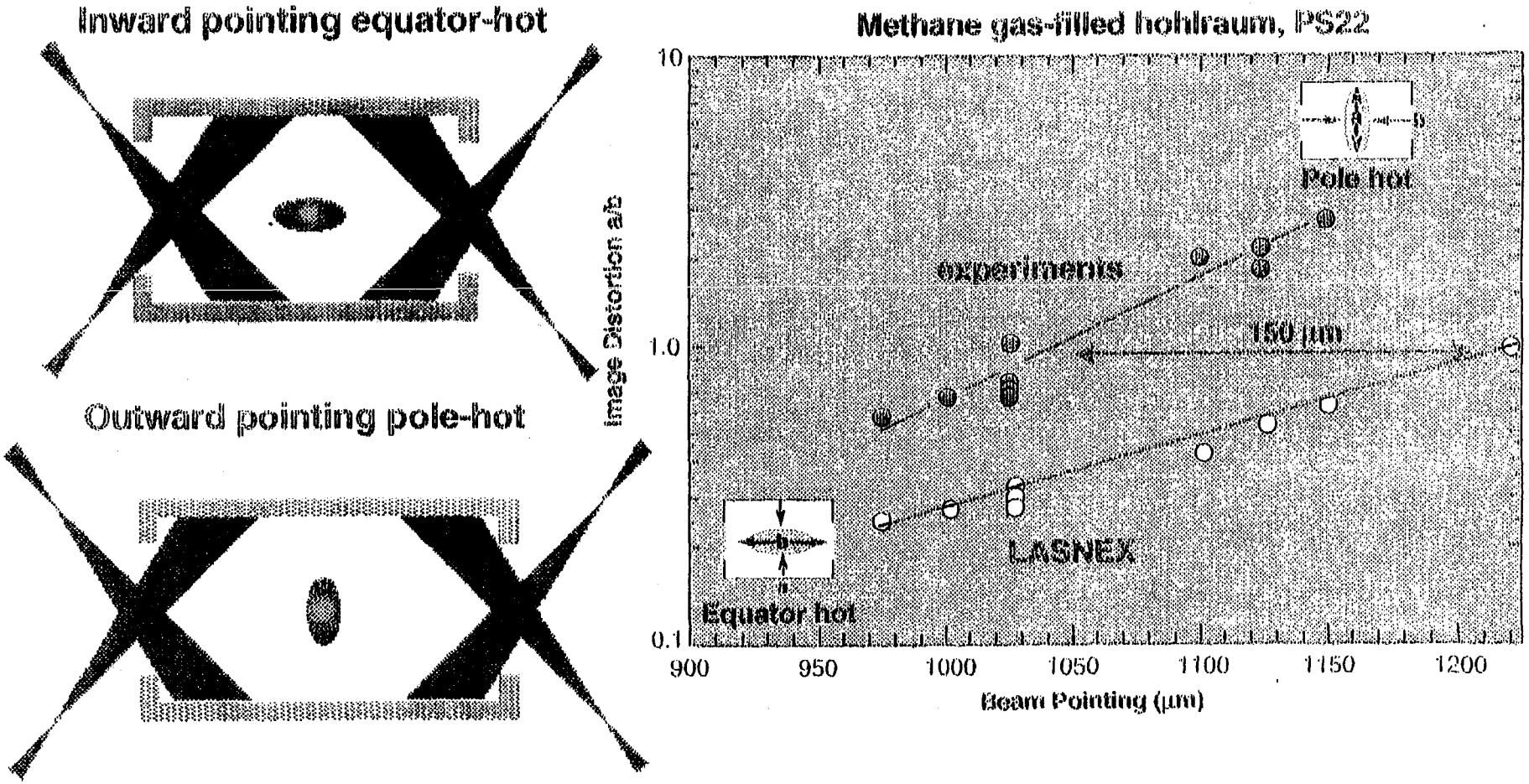
Inward pointing equator-hot
Outward pointing pole-hot
Image Distortion a/b
Methane gas-filled hohlraum, PS22
10
1.0
0.1
900
950
1000
1050
1100
1150
1200
Beam Pointing (μm)
Pole hot
experiments
150 μm
LASNEX
Equator hot

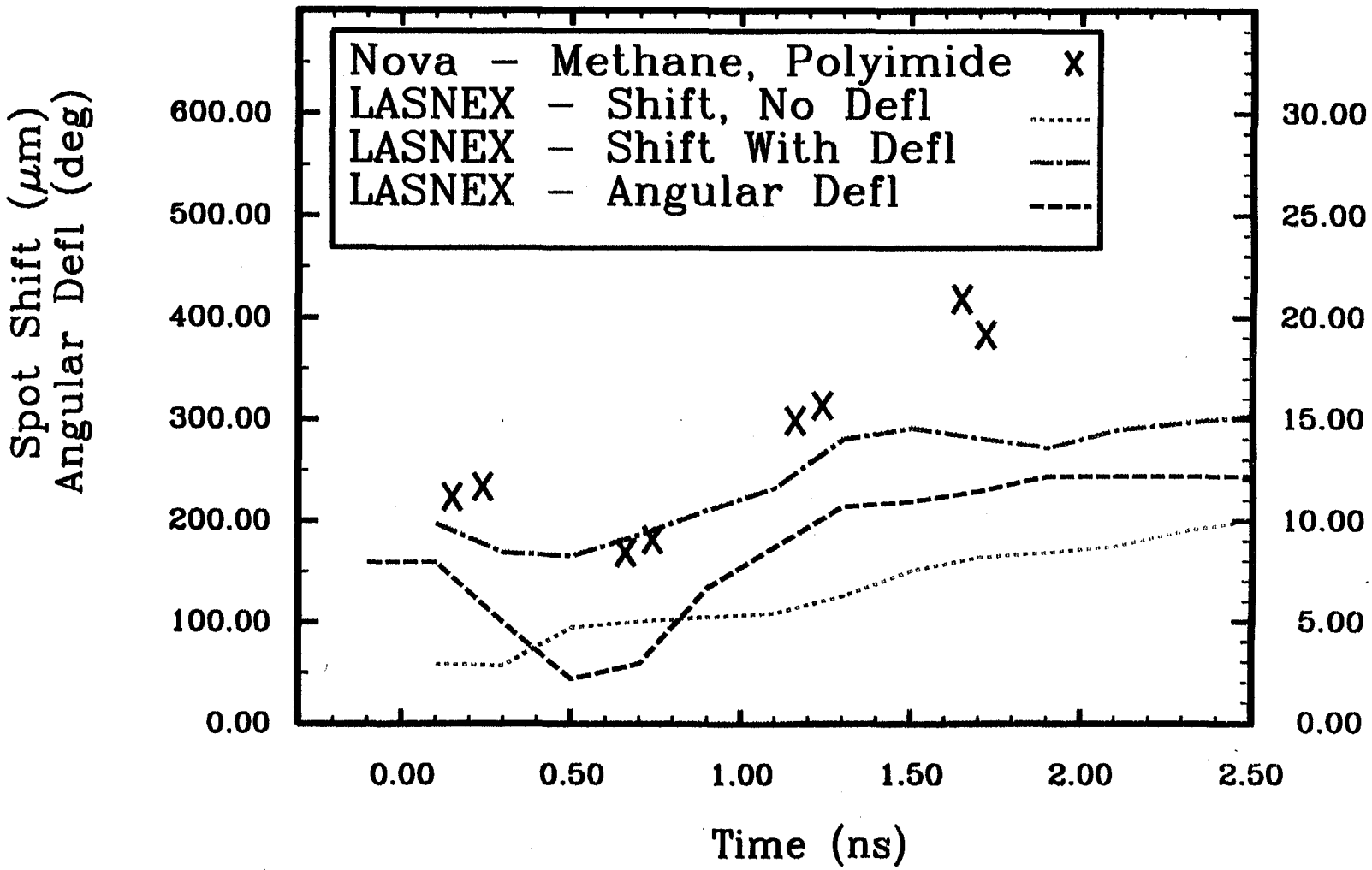
Nova – Methane, Polyimide x
LASNEX – Shift, No Defl
LASNEX – Shift With Defl
LASNEX – Angular Defl
Spot Shift (μm)
Angular Defl (deg)
600.00
500.00
400.00
300.00
200.00
100.00
0.00
30.00
25.00
20.00
15.00
10.00
5.00
0.00
0.00
0.50
1.00
1.50
2.00
2.50
Time (ns)

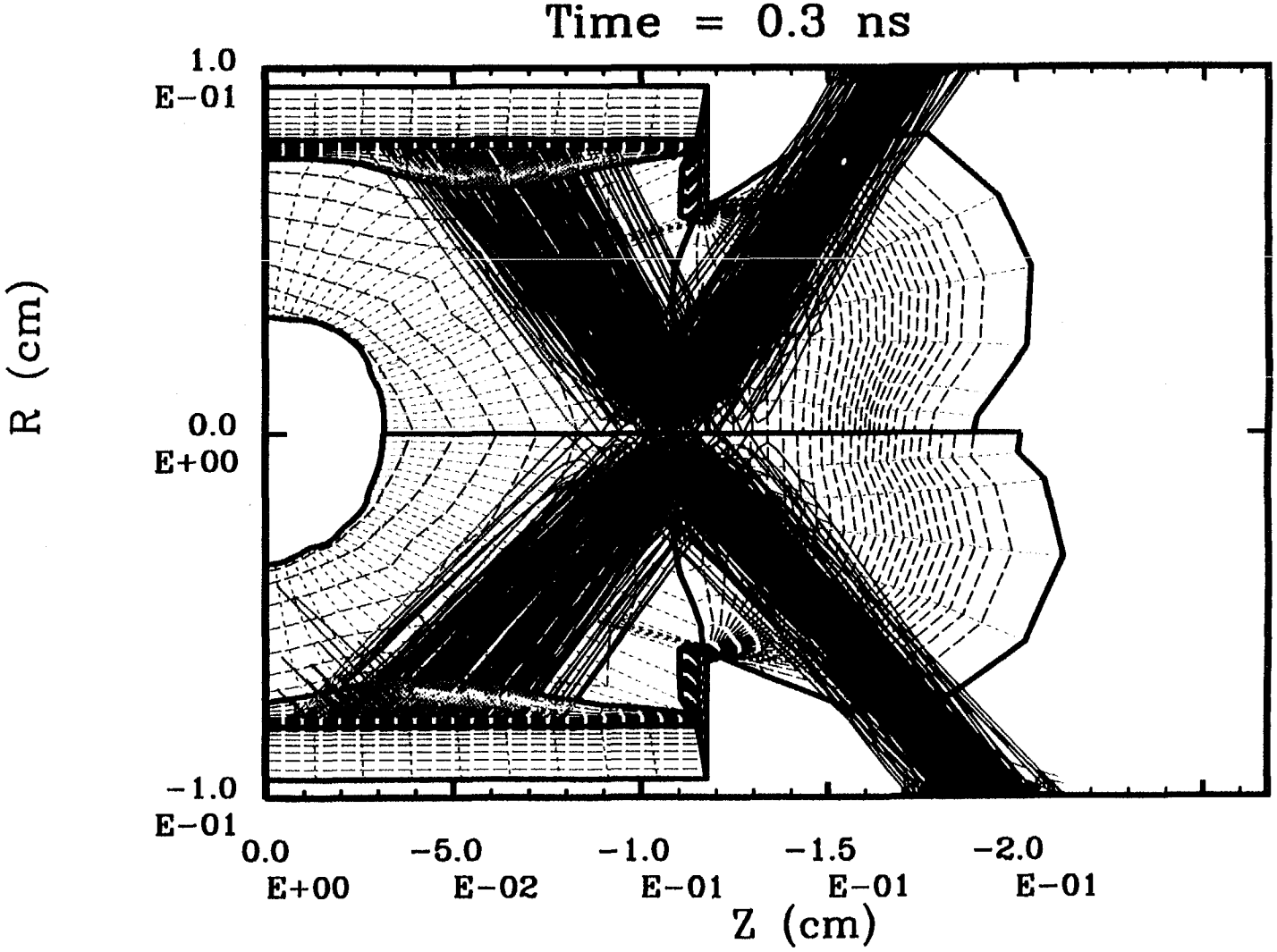
Time = 0.3 ns
1.0
E-01
0.0
E+00
-1.0
E-01
R (cm)
0.0
E+00
-5.0
E-02
-1.0
E-01
-1.5
E-01
-2.0
E-01
Z (cm)

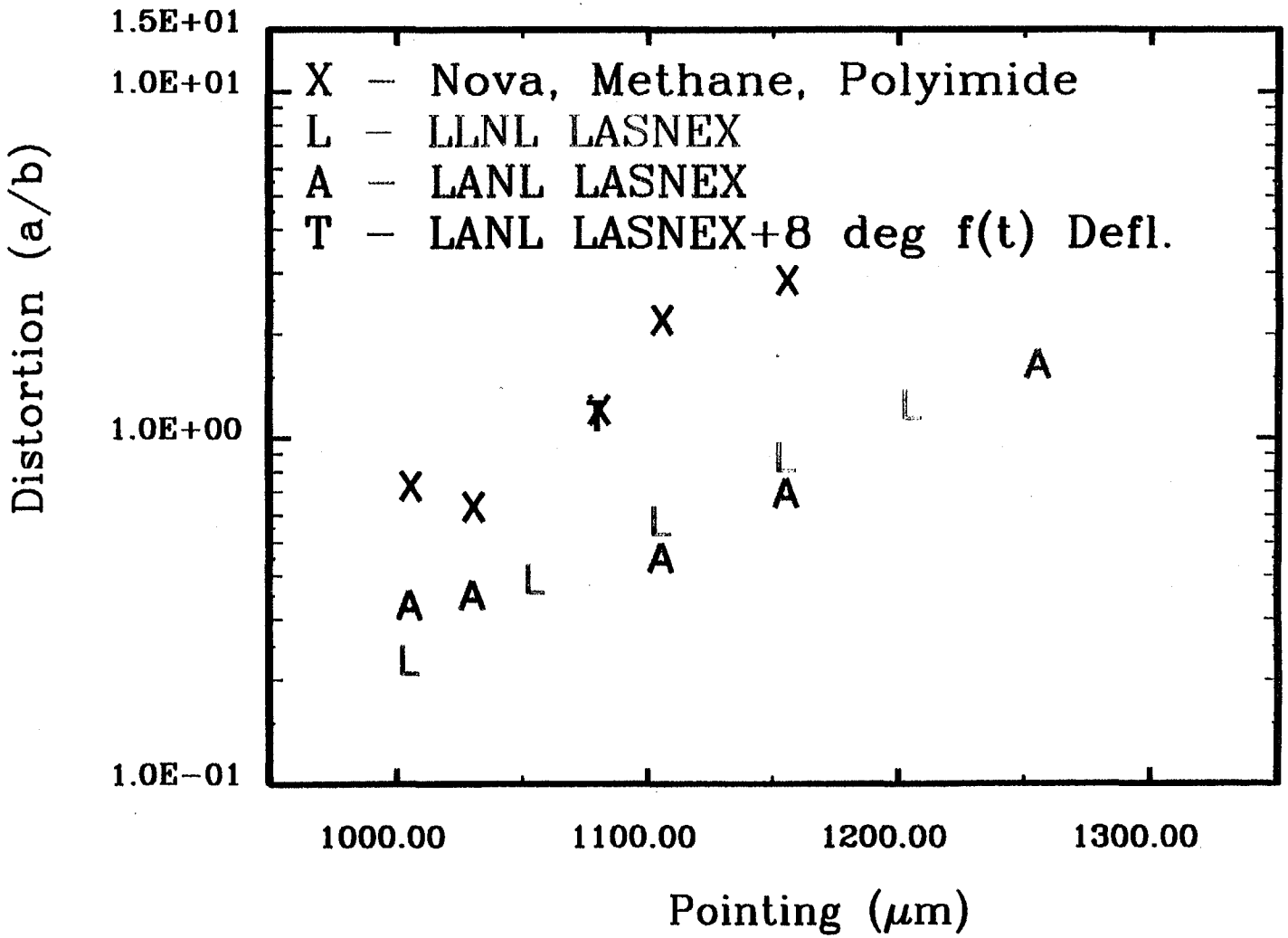
X – Nova, Methane, Polyimide
L – LLNL LASNEX
A – LANL LASNEX
T – LANL LASNEX+8 deg f(t) Defl.
1.5E+01
1.0E+01
1.0E+00
1.0E−01
Distortion (a/b)
1000.00
1100.00
1200.00
1300.00
Pointing (μm)

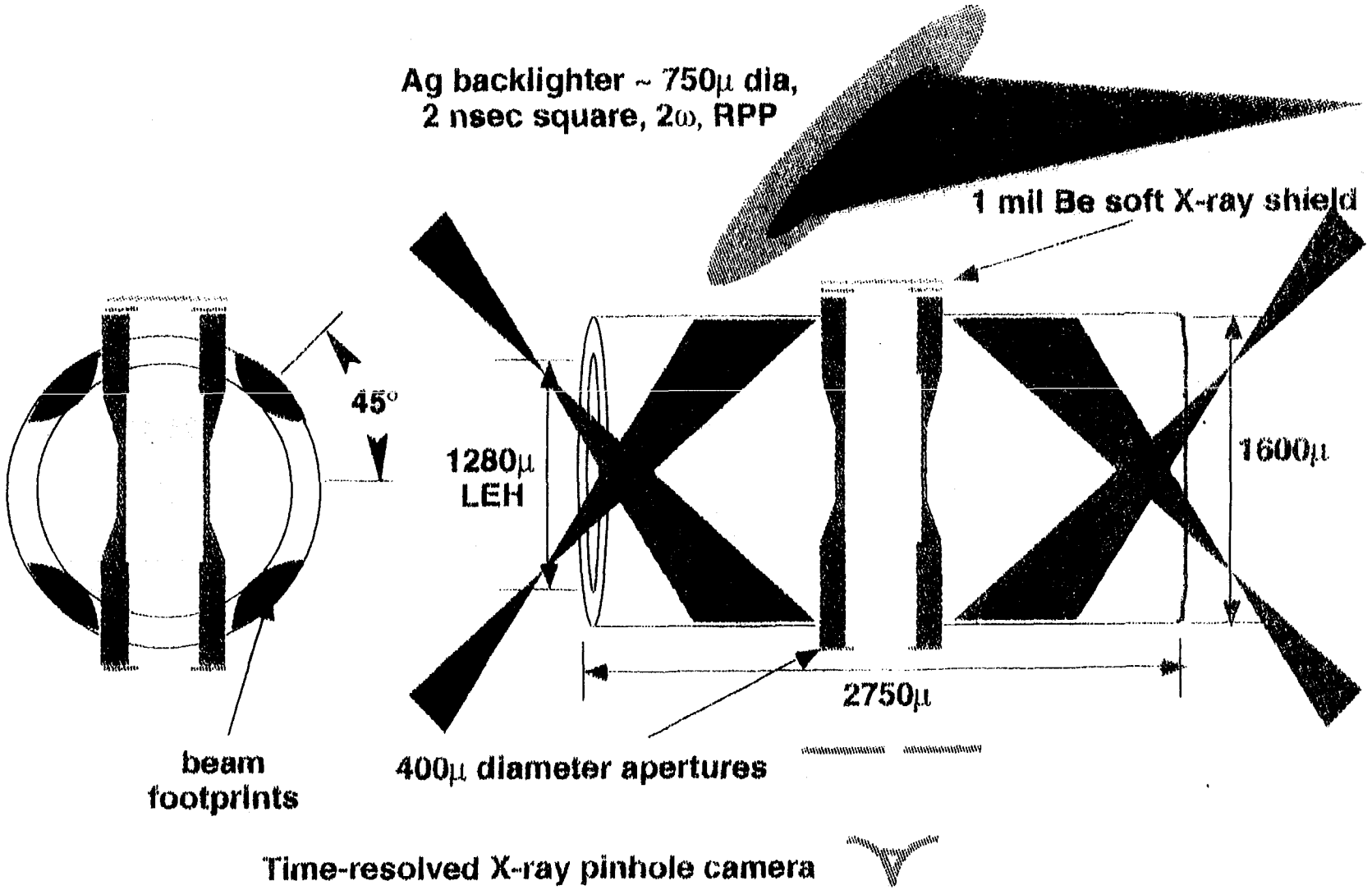

Time-resolved X-ray pinhole camera

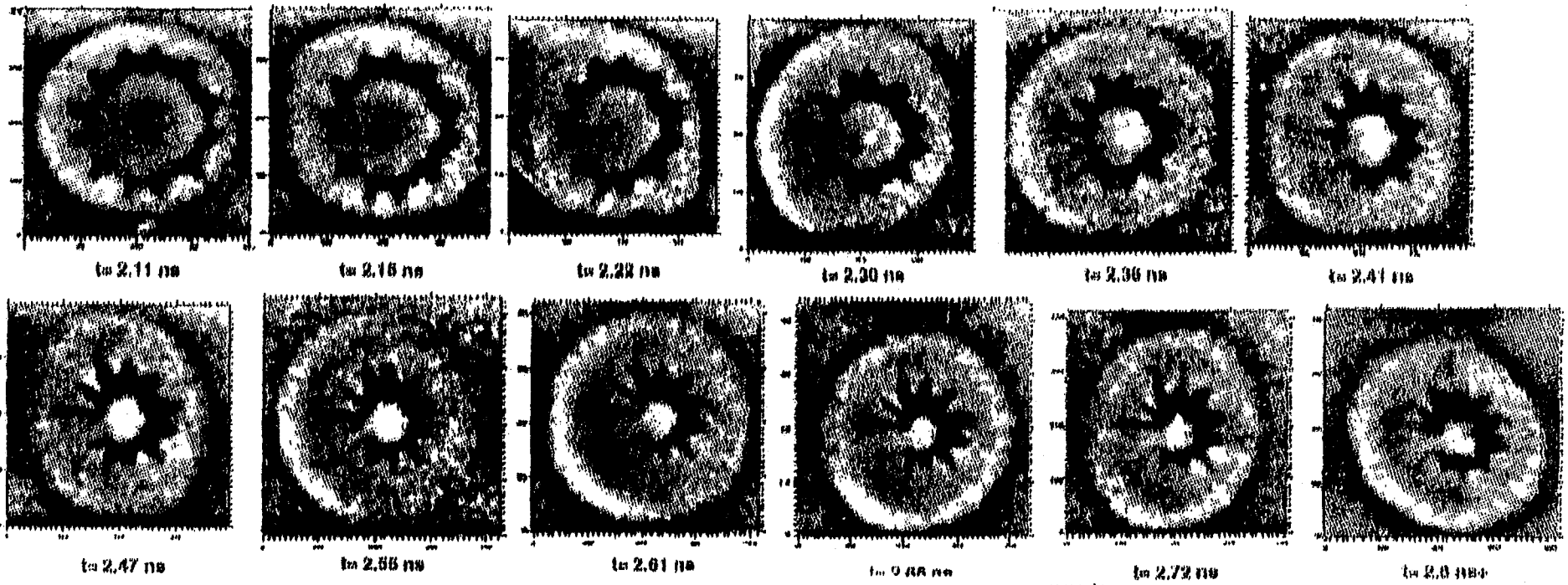

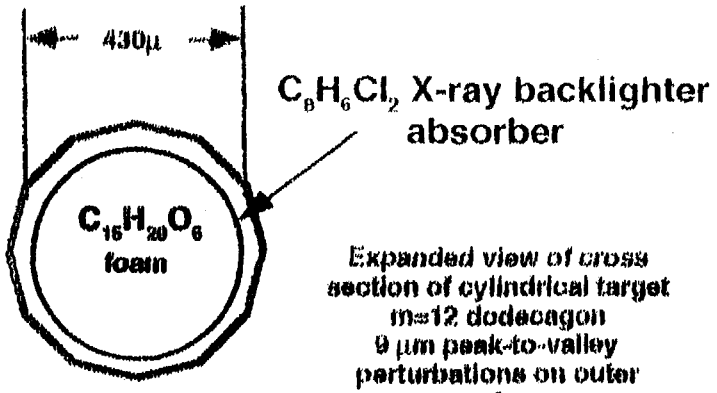

Expanded view of cross section of cylindrical target
m=12 dodecagon
9 μm peak-to-valley perturbations on outer surface

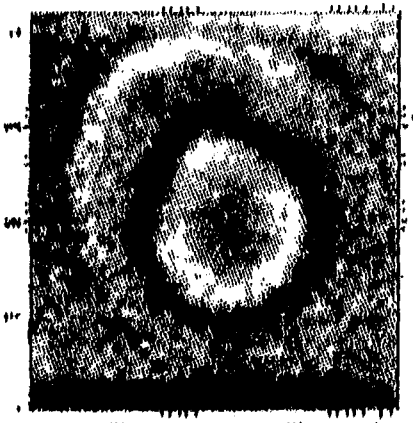

unperturbed
t = 2.16 nsec,

- **No growth is observed with a smooth outer surface**

139 μm D-T Solid Layer & Empty Cell Power Spectra